Origin of the Magnetoelectric Coupling Effect in $Pb(Zr_{0.2}Ti_{0.8})O_3/La_{0.8}Sr_{0.2}MnO_3$ Multiferroic Heterostructures

C. A. F. Vaz,[1,*] J. Hoffman,[1] Y. Segal,[1] J. W. Reiner,[1] R. D. Grober,[1] Z. Zhang,[2] C. H. Ahn,[1] and F. J. Walker[1]

[1]*Department of Applied Physics and CRISP, Yale University, New Haven, Connecticut 06520, USA*

[2]*Advanced Photon Source, Argonne National Laboratory, Argonne, Illinois 60439, USA*

(Received 17 December 2009; published 25 March 2010)

The electronic valence state of Mn in $Pb(Zr_{0.2}Ti_{0.8})O_3/La_{0.8}Sr_{0.2}MnO_3$ multiferroic heterostructures is probed by near edge x-ray absorption spectroscopy as a function of the ferroelectric polarization. We observe a temperature independent shift in the absorption edge of Mn associated with a change in valency induced by charge carrier modulation in the $La_{0.8}Sr_{0.2}MnO_3$, demonstrating the electronic origin of the magnetoelectric effect. Spectroscopic, magnetic, and electric characterization shows that the large magnetoelectric response originates from a modified interfacial spin configuration, opening a new pathway to the electronic control of spin in complex oxide materials.

DOI: 10.1103/PhysRevLett.104.127202 PACS numbers: 75.70.Cn, 73.90.+f, 75.60.Ej, 78.70.Dm

Understanding how to couple the electric and magnetic order parameters in the solid state is a long-standing scientific challenge that is intimately linked to the spatial and temporal symmetries associated with charge and spin. Coupling of the order parameters is observed in many different materials, but the effect is generally weak in magnitude, even in materials that are both ferroelectric and ferromagnetic (*multiferroic*) [1–3]. Increasing the magnitude of the coupling is a fundamental problem in condensed matter physics with important implications for applications. For example, strong magnetoelectric coupling allows for the ultrasensitive measurement of weak magnetic fields, and at smaller length scales, enables spin-based technologies by allowing the control of the spin state at the atomic scale via electric fields.

In single phase multiferroics, the magnetic and ferroelectric orders often occur largely independent of each other, and as a result, the magnetoelectric coupling tends to be small [2,4]. In order to overcome this intrinsic limitation in the coupling between the order parameters, artificially structured materials with enhanced magnetoelectric couplings have been engineered, where a break in time reversal and spatial symmetry occurs naturally at the interface between the different phases [3,5,6]. Moreover, the coupling mechanism can be tailored to benefit from several phenomena, including elastic [7,8], magnetic exchange bias [9–11], and charge-based [12] couplings. In charge-based multiferroic composites, the sensitivity of the electronic and spin state of strongly correlated oxides to charge provides enhanced coupling between magnetic and ferroelectric order parameters [12]; it often relies on charge doping of a ''colossal'' magnetoresistive (CMR) manganite to modulate between high and low spin states, which compete for the ground state of the system. However, the microscopic origin of this effect is still not fully understood. In particular, the nature of the effect and how the interplay between charge, spin, and valency combines to yield the large magnetoelectric response in this system remain to be addressed. In this Letter, we explore the sensitivity of x-ray absorption near edge spectroscopy (XANES) to the atomic electronic state to demonstrate the microscopic origin of the magnetoelectric effect found in $Pb(Zr_{0.2}Ti_{0.8})O_3/La_{0.8}Sr_{0.2}MnO_3$ (PZT/LSMO) heterostructures. XANES is particularly sensitive to changes in the atomic valence state, and therefore especially suited to probing charge-induced changes in the atomic structure of LSMO; another advantage is the ability to probe buried layers. Direct quantification of the charge-driven magnetic changes based on the spectroscopic, electric, and magnetic measurements show that both the spin state and spin configuration of LSMO are modulated, whereby the interfacial spin coupling changes from ferromagnetic to antiferromagnetic, giving rise to the large magnitude of the magnetoelectric effect found in this system. A similar interfacial magnetic reconstruction effect is also predicted from first principles calculations in similar type of heterostructures [13].

The samples in this study consist of 250 nm $Pb(Zr_{0.2}Ti_{0.8})O_3/t\,La_{0.8}Sr_{0.2}MnO_3/SrTiO_3(001)$ epitaxial heterostructures with $t = 11$, 12 unit cells (u.c.), grown on TiO_2-terminated $SrTiO_3$ substrates. At the doping level chosen ($x = 0.2$), the bulk LSMO system lies near the boundary between insulating and metallic ferromagnetic ground states [14,15]. Two films were grown simultaneously for each thickness, one on an unpatterned $SrTiO_3$ substrate and another on a TiO_x-masked substrate, exposing two identical Hall-bar device structures defined by optical lithography. The active area is $160 \times 320\ \mu m^2$ [Fig. 1(c), inset]. The LSMO films are grown by molecular beam epitaxy in an ultrahigh vacuum deposition system with a base pressure of 1×10^{-10} mbar. The elemental materials are evaporated from effusion cells under a O_2 partial pressure of 1×10^{-7} mbar, with the substrates held at 720 °C. The evaporation rates are determined for each material from a calibrated thickness monitor (2% error), while film thickness is monitored in real time using reflec-

tion high energy electron diffraction (RHEED) intensity oscillations. The observation of the latter indicates that film growth occurs in a layer-by-layer mode; atomic force microscopy of LSMO films shows the presence of unit cell high steps separating large, flat terraces [Fig. 1(b), inset]. After the LSMO deposition, the samples are cooled to room temperature in 1×10^{-7} mbar of O_2 and then transferred to an off-axis RF sputtering system for PZT deposition using the conditions described in Ref. [16]. The LSMO films studied here have the minimum thickness for which a peak in resistivity is observed [17]; we focus here on the results obtained for 12 u.c. structures, which are representative of all measurements. The direction of the PZT polarization is used to modulate electrostatically the hole-carrier density in the LSMO (hole charge depletion occurs when the PZT polarization points down into the LSMO film, and hole accumulation in the opposite case).

The XANES measurements were carried out at Beamline 33-ID of the Advanced Photon Source, Argonne National Laboratory (Illinois). A monochromatic x-ray beam 300×120 μm^2 in size (defined using slits) was set perpendicular to the sample and aligned onto the gate electrode of the device within 10 μm using the measured x-ray induced photocurrent. The sample was mounted in an evacuated variable temperature Displex cryostat equipped with a Be dome. In this experiment, we probe the absorption K edge of Mn, corresponding to the allowed electric dipole transition from the $1s$ core level to unoccupied $4p$ states [18–20]. The light absorption, normalized to the incident photon flux, was measured in the fluorescence mode using the Mn $K\alpha$ line at 5899 eV using a Si drift x-ray detector spectrometer. Several scans were performed on multiple device structures, including scan cycles where the PZT was switched consecutively at each energy value (gate voltage set to ± 5 V). Scans were also carried out where the x-ray absorption was measured at a fixed energy as a function of the gate voltage. A reference x-ray absorption spectrum of metallic Mn was taken for energy calibration.

The results of the electrical, transport, and magnetic property measurements of the PZT/LSMO structure are shown in Fig. 1. The electrical switching properties of the PZT gate dielectric at room temperature, Fig. 1(a), show abrupt switching of the ferroelectric polarization. From integration of the displacement current, we obtain a saturation polarization of $P_s = 85$ $\mu C/cm^2$. Transport characteristics are shown in Fig. 1(b) for both states of the PZT polarization at a magnetic field of 0 and 50 kOe, applied out of plane. The peak in resistivity marks the transition between metallic and insulating states, and is found to change by ~40 K, from 188 K in the depletion state to 226 K in the accumulation state. The presence of a magnetic field leads to an increase in the resistivity peak temperature, which is responsible for the CMR effect in the doped manganites [14,21]. The magnetic behavior was probed with magneto-optic Kerr-effect (MOKE) magnetometry as described in Ref. [12]. Magnetization versus temperature measurements show a change in critical temperature of 20 K, from 180 K in the depletion state to 200 K in the accumulation state, showing that the peak in resistivity, although correlated to the onset of magnetic order, does not coincide exactly with the magnetic critical temperature [22]. These results show that both the transport and magnetic properties can be modulated electrostatically via the ferroelectric field effect. For magnetic hysteresis loops measurements, the magnetic field was varied linearly at a rate of 1 Hz, and a gate voltage of ± 10 V was used to switch the PZT polarization. The results are plotted in Fig. 1(c) for the two polarization states of PZT (100 K). The data show that the accumulation state has a smaller saturation magnetization than the depletion state, in agreement with previous results [12]. To obtain a quantitative estimate of the change in magnetization, we carried out SQUID magnetometry on the unpatterned PZT/LSMO

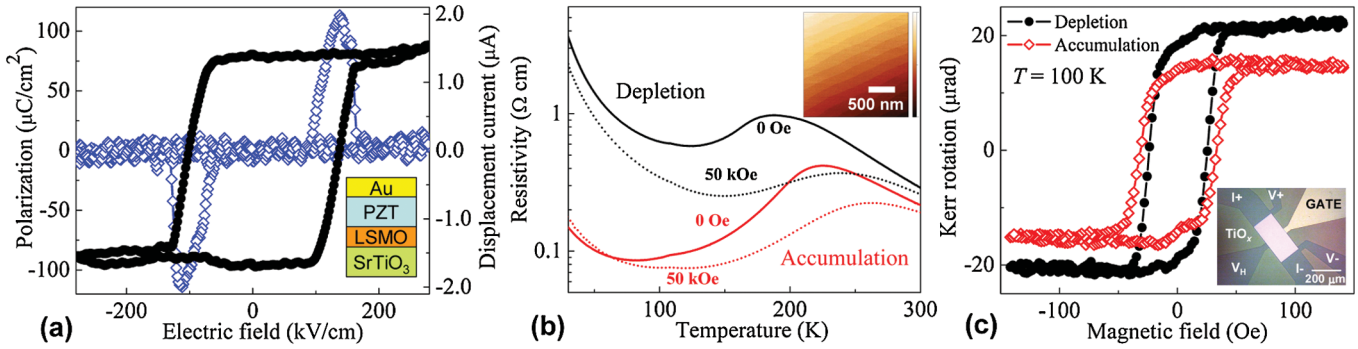

FIG. 1 (color). Electric, transport, and magnetic behavior of the PZT/12 u.c. LSMO structure, showing: (a) Room temperature polarization-electric field loop (full circles) and displacement current (empty diamonds) of PZT. Inset: cross sectional schematic of the sample structure. (b) Resistivity versus temperature curves for both the accumulation (red) and depletion (black) states at zero and at 50 kOe applied magnetic field. Inset: atomic force microscopy image of a 20 nm LSMO film (vertical scale range is 12 nm). (c) Magnetic hysteresis curves of LSMO along the in-plane ⟨100⟩ direction for the two polarization states of PZT, taken at 100 K (averages of ~300 individual traces). Inset: optical image of the device before Au metallization; I +, I −, V +, V− denote the current and voltage contacts for the resistivity measurements.

sample, giving a saturation magnetization of 515 emu/cm^3, or $m_{dep} = 3.30\mu_B$/Mn. Piezoelectric force microscopy of the unpatterned film shows that the electric polarization state of the PZT after growth points down; hence, this value of the magnetic moment corresponds to the LSMO in the depletion state. From the ratio $m_{dep}/m_{acc} = 1.30(3)$ obtained from MOKE, we estimate the magnetic moment for the accumulation state as $m_{acc} = 2.54(6)\mu_B$/Mn, giving a change in magnetic moment of $\Delta m = m_{dep} - m_{acc} = 0.76(6)\mu_B$/Mn. From these data, we obtain a magnetoelectric coupling coefficient of $\Delta M/\Delta E = 6.2 \times 10^{-3}$ Oe cm V^{-1} at 100 K.

The key experimental results of this work are the XANES data plotted in Fig. 2, showing the room temperature x-ray absorption response for the two states of the PZT polarization. The main finding is the observation of an energy shift in the Mn absorption edge by +0.3 eV upon switching the PZT polarization from the depletion to the accumulation state. The position of the absorption edge is very sensitive to the cationic valency in a wide array of compounds [23]. In the case of the manganites, the energy edge position is found to vary with the doping level x by about 3.5 eV in $LaMn_{1-x}Co_xO_3$ [24], 3–4.2 eV in $La_{1-x}Ca_xMnO_3$ [18–20], 2.5–3 eV in $La_{1-x}Sr_xMnO_3$ [25,26], along with other more subtle changes in peak amplitude and edge shape. The edge energy position increases from the metallic state (Mn^0) to higher formal valence states, and the observation of an energy shift between the depletion and accumulation states shows directly a change in the average Mn valency induced by the electrostatic hole-carrier modulation. This change in the valency of the Mn is responsible for the changes in the magnetic state of LSMO [Fig. 1(c)] and lies at the origin of the large magnetoelectric effect [12]. Importantly, in these measurements, no change in the crystal lattice occurs. Measurements at low temperature (20 K) display a similar change in the Mn valency, showing that the charge carrier modulation is robust and occurs independent of temperature [Fig. 2(b)]. The difference spectrum between depletion and accumulation states is shown in Fig. 2(b), which is reproduced well at the absorption edge by a single parameter model corresponding to a rigid shift in energy of 0.3 eV between the averaged absorption spectra. A more direct visualization of the valence modulation can be seen in Fig. 2(c), which shows the x-ray absorption as a function of the applied gate voltage at fixed photon energy, showing that the x-ray absorption can be modulated between a high and a low value as the PZT polarization is switched. This result mimics the P-E hysteresis curve [Fig. 1(b)] and demonstrates that the change in Mn valency tracks the switching of the PZT polarization.

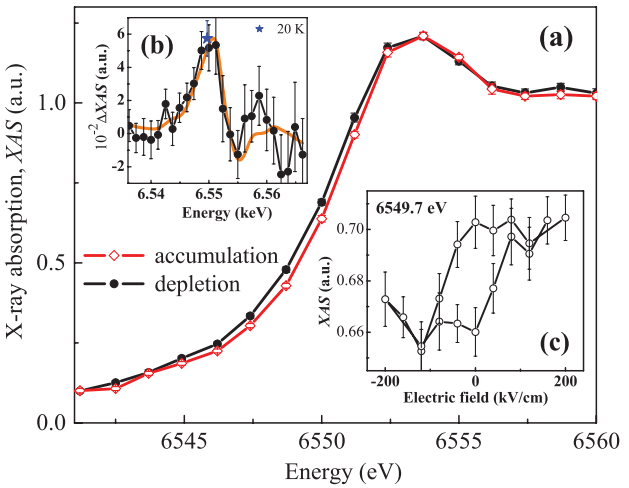

FIG. 2 (color). (a) Room temperature XANES results for the two polarization states of the PZT. (b) Difference in x-ray absorption for the two PZT polarization states; the full line models this difference assuming a rigid shift in the Mn absorption edge. (c) Variation of the x-ray light absorption as a function of the applied gate voltage at a fixed energy, $E = 6549.7$ eV. The error bars reflect counting statistics.

We may estimate the change in the Mn valency from XANES spectra for the chemically doped LSMO compounds [25,26]. From the results by Shibata *et al.* [25] showing a linear variation in the energy shift with the formal average valency of Mn, $\Delta E = 3.0x$, we estimate an averaged change in Mn valency of $\Delta x = 0.1$/Mn between the accumulation and depletion states. The relative change in the surface charge polarization of PZT, of $2P_s = 1.6\ e$/u.c.^{2}, corresponds to a change in charge of $\Delta n = 0.13$/Mn. The agreement is striking and shows that most surface charge is screened by charge carriers from the LSMO. This change in valency is expected to take place mostly at the PZT/LSMO interface, within the screening length of LSMO of about 1 u.c. [17].

One can now correlate the observed changes in the magnetization with the valence modulation. Since going from the high spin state Mn^{3+} ($S = 2$) to the low spin state Mn^{4+} ($S = 3/2$) changes the magnetic moment by $1\mu_B$, the measured change in Mn valency gives a change in moment of $0.1\mu_B$/Mn between the depletion and accumulation states. Such a change is much smaller than the measured change in magnetic moment of $\Delta m = 0.76(6)\mu_B$/Mn. Hence, the change in magnetic moment, equivalent to about 2 u.c., must be explained by a mechanism other than the change in the spin state of Mn induced by the valency modulation. Instead, the change in moment must originate from a modification in the spin exchange coupling at the interface, for example, from ferromagnetic in the depletion state to antiferromagnetic in the accumulation state, whereby the spins couple ferromagnetically within this interfacial layer and antiferromagnetically with the spins of the (001) adjacent layers. Such spin arrangement has been recently calculated to be favored for the accumulation state of $La_{0.5}Ba_{0.5}MnO_3/BaTiO_3$ multiferroic heterostructures [13]. Our results provide an experimental signature of the magnetic interface reconstruction occurring at the PZT/LMSO interface. A model depicting the magnetic reordering is shown in Fig. 3. In this picture, the interface layer in the accumulation state consists of

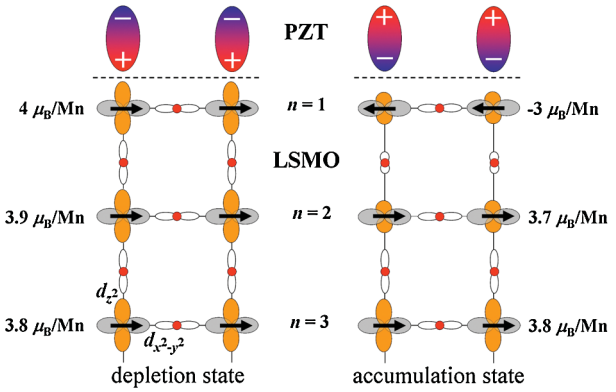

FIG. 3 (color). Schematic model of the spin configurations in LSMO at the PZT interface for the depletion and accumulation states, showing the changes in the Mn and O orbital states and the expected changes in the magnetic moment per layer. The arrows indicate the spin orientation in the Mn cations and n denotes the unit cell number below the PZT. The Mn d orbitals are drawn in orange and grey, and the lobes of the p orbitals are shown around the oxygen atoms (red).

strongly depopulated antibonding e_g $3z^2 - r^2$ states, weakening the double-exchange interaction at these orbitals; an antiferromagnetic coupling to the adjacent layers would then ensue if the $x^2 - y^2$ orbitals are energetically favored (favoring the superexchange interaction). This result is predicted by first-principles calculations for LSMO under tensile strain, where a ferromagnetic coupling is favored at low doping levels and antiferromagnetic alignments are favored at higher doping [27]. This change in spin configuration results in a change in the average moment of $(4 + 3 + 0.2)/12 = 0.6\mu_B$/Mn between depletion and accumulation states (see Fig. 3), which is close to the observed value. This result also agrees with the trend observed in the bulk phase diagram, where an antiferromagnetic coupling of alternating (001) planes is favored for hole doping between 0.5 and 0.65 at low temperatures [14,15]. This mechanism gives rise to a much more dramatic change in the average magnetic moment and explains the very large magnetoelectric coupling [12,13].

In summary, we have demonstrated via x-ray absorption spectroscopy the electronic origin of the magnetoelectric coupling in PZT/LSMO multiferroic heterostructures, which arises from a change in the valence state of Mn induced by electrostatic charge modulation. The XANES data provide a direct and quantitative measure of the changes in the number of electrons populating the Mn $3d$ e_g bands, which are responsible for the magnetic behavior of the LSMO. We conclude that the large magnetoelectric coupling effect found in these artificial heterostructures results from an interfacial magnetic reconstruction driven by charge accumulation. These findings show a new pathway to the electronic control of spin in complex oxide materials.

The authors acknowledge financial support by the NSF through MRSEC DMR 0520495 (CRISP), FENA, and the NRI. Use of the Advanced Photon Source was supported by the DOE, Office of Science, Office of Basic Energy Sciences, under Contract No. DE-AC02-06CH11357.

*Corresponding author. carlos.vaz@yale.edu

[1] H. Schmid, Ferroelectrics **162**, 317 (1994).
[2] N. A. Hill, J. Phys. Chem. B **104**, 6694 (2000).
[3] R. Ramesh and N. A. Spaldin, Nature Mater. **6**, 21 (2007).
[4] D. I. Khomskii, Physics **2**, 20 (2009).
[5] W. Eerenstein, N. D. Mathur, and J. F. Scott, Nature (London) **442**, 759 (2006).
[6] J. M. Rondinelli, M. Stengel, and N. A. Spaldin, Nature Nanotech. **3**, 46 (2008).
[7] M. Fiebig, J. Phys. D **38**, R123 (2005).
[8] C. Thiele, K. Dörr, O. Bilani, J. Rödel, and L. Schultz, Phys. Rev. B **75**, 054408 (2007).
[9] P. Borisov, A. Hochstrat, X. Chen, W. Kleemann, and C. Binek, Phys. Rev. Lett. **94**, 117203 (2005).
[10] V. Laukhin *et al.*, Phys. Rev. Lett. **97**, 227201 (2006).
[11] Y.-H. Chu *et al.*, Nature Mater. **7**, 478 (2008).
[12] H. J. A. Molegraaf, J. Hoffman, C. A. F. Vaz, S. Gariglio, D. van der Marel, C. H. Ahn, and J.-M. Triscone, Adv. Mater. **21**, 3470 (2009).
[13] J. D. Burton and E. Y. Tsymbal, Phys. Rev. B **80**, 174406 (2009).
[14] M. Imada, A. Fujimori, and Y. Tokura, Rev. Mod. Phys. **70**, 1039 (1998).
[15] O. Chmaissem, B. Dabrowski, S. Kolesnik, J. Mais, J. D. Jorgensen, and S. Short, Phys. Rev. B **67**, 094431 (2003).
[16] X. Hong, A. Posadas, A. Lin, and C. H. Ahn, Phys. Rev. B **68**, 134415 (2003).
[17] X. Hong, A. Posadas, and C. H. Ahn, Appl. Phys. Lett. **86**, 142501 (2005).
[18] M. Croft, D. Sills, M. Greenblatt, C. Lee, S.-W. Cheong, K. V. Ramanujachary, and D. Tran, Phys. Rev. B **55**, 8726 (1997).
[19] G. Subías, J. García, M. G. Proietti, and J. Blasco, Phys. Rev. B **56**, 8183 (1997).
[20] F. Bridges, C. H. Booth, M. Anderson, G. H. Kwei, J. J. Neumeier, J. Snyder, J. Mitchell, J. S. Gardner, and E. Brosha, Phys. Rev. B **63**, 214405 (2001).
[21] E. L. Nagaev, Phys. Rep. **346**, 387 (2001).
[22] S. E. Lofland, S. M. Bhagat, K. Ghosh, R. L. Greene, S. G. Karabashev, D. A. Shulyatev, A. A. Arsenov, and Y. Mukovskii, Phys. Rev. B **56**, 13705 (1997).
[23] P. P. Kirichok, A. V. Kopaev, and V. P. Pashchenko, Russ. Phys. J. **28**, 849 (1985).
[24] M. Sikora, C. Kapusta, K. Knížek, Z. Jirák, C. Autret, M. Borowiec, C. J. Oates, V. Procházka, D. Rybicki, and D. Zajac, Phys. Rev. B **73**, 094426 (2006).
[25] T. Shibata, B. A. Bunker, and J. F. Mitchell, Phys. Rev. B **68**, 024103 (2003).
[26] R. Bindu, S. K. Pandey, A. Kumar, S. Khalid, and A. V. Pimpale, J. Phys. Condens. Matter **17**, 6393 (2005).
[27] Z. Fang, I. V. Solovyev, and K. Terakura, Phys. Rev. Lett. **84**, 3169 (2000).